Applied Thermal Engineering 87 (2015) 595–604

Contents lists available at ScienceDirect

Applied Thermal Engineering

journal homepage: www.elsevier.com/locate/apthermeng

Research paper

The electro-spraying characteristics of ethanol for application in a small-scale combustor under combined electric field

Yunhua Gan [a, b, *], Zhibin Luo [a, b], Yongpan Cheng [c], Jinliang Xu [c, **]

[a] School of Electric Power, South China University of Technology, Guangzhou, 510640, China
[b] Guangdong Province Key Laboratory of Efficient and Clean Energy Utilization, South China University of Technology, Guangzhou, 510640, China
[c] The Beijing Key Laboratory of Multiphase Flow and Heat Transfer, North China Electric Power University, Beijing, 102206, China

HIGHLIGHTS

- Pulsed-jet, cone-jet, skewed cone-jet, and multi-jet were observed.
- Different electro-spraying modes for ethanol were divided into several regions.
- The driving force in jet region came from the electrostatic induction field.
- The electric field supplied driving force for the motion of liquid droplets.
- The specific charges of ethanol reached maximum value at the cone-jet mode.

ARTICLE INFO

Article history:
Received 5 February 2015
Accepted 24 May 2015
Available online 30 May 2015

Keywords:
Electro-spraying
Micro-scale combustion
Cone-jet mode
Specific charge

ABSTRACT

A small-scale combustor with electro-spraying technique was investigated. It consisted of vertical quartz glass tubes with an inner diameter of 16.0 mm. A stainless steel ring and a stainless steel mesh were used as an extractor and a collector, respectively. A capillary tube with an inner diameter of 0.9 mm was used as a nozzle. The nozzle and the steel ring were connected to the positive electrode of Direct Current power sources. The steel mesh was the droplets collector and a flame holder. Stable combustion flame was observed under combined electric fields. The electro-spraying modes of pulsed-jet, cone-jet, skewed cone-jet, and multi-jet were observed. The operating ranges were divided into several regions at various voltages and flow rates. The whole fluid field was divided into the jet region and spraying region. The driving force in the jet region came from the electrostatic induction field between the nozzle and the steel ring. The electric field between the steel ring and steel mesh supplied the driving force to move liquid droplets in the spraying region. The steel mesh is a key component for the directional movement of liquid droplets. Taylor angles measured at cone-jet mode were in the range of 75.18°–82.45°.

1. Introduction

In recent years, liquid electro-spraying has been a hot topic with growing interest due to its wide applications in such areas as fuel atomization in combustion systems [1,2], cooling for microelectronics [3–5], electro spinning process [6,7], deposition of thin functional films [8] and other areas [9–11]. There are some other researches on charge injection atomizers using dielectric liquid only [12–14]. In present study, we aim at the micro combustor applying electro-spraying technique and using liquid ethanol with low conductivity as fuel.

The crucial component in a micro energy system is the micro-combustor with stable flames, but it is very difficult to keep flames stable in the micro-combustor, due to short residence time and high heat loss rate [15–17]. Combustion using liquid hydrocarbon fuels can supply relatively high energy density but bring more challenges [18]. Electro-spraying is an ideal method in micro-scale combustion system with liquid fuels.

Kyritsis et al. [19] presented a meso-scale catalytic combustor coupled with direct energy conversion modules for power production. The jet fuelJP8 (Jet Propellant 8) was electro-sprayed at a flow rate on the order of 10 g/h and combusted under the equivalence ratios varying from 0.35 to 0.70 with estimated combustion

* Corresponding author. Tel.: +86 20 87110613.
** Corresponding author. Tel.: +86 10 61772163.
E-mail addresses: ganyh@scut.edu.cn (Y. Gan), xjl@ncepu.edu.cn (J. Xu).

http://dx.doi.org/10.1016/j.applthermaleng.2015.05.046
1359-4311/

Nomenclature

A_q	specific charge(C/kg)
E	electric field strength(kV/m)
E_a	axial electric field strength(kV/m)
E_r	radial electric field strength(kV/m)
F	electrical field force(N)
L_1	distance from the outlet of the capillary nozzle to the steel ring(mm)
L_2	distance from the steel ring to the steel mesh(mm)
I	current (A)
I_0	initial current (A)
m	mass flux of liquid ethanol (kg/s)
m_1	mass flux of liquid ethanol evaporated into the air (kg/s)
P_{in}	internal pressure(N)
P_{ex}	external pressure(N)
Q_v	flow rate(ml/h)
R	resistance (MΩ)
r	radius of jet(mm); polar coordinates (mm)
r_{cr}	critical radius of jet(mm)
t	measurement period (s)
U	electric potential difference (mV)
V_1	voltage on the capillary nozzle(kV)
V_2	voltage on the steel ring(kV)

Greek symbols

ε_0	permittivity of air(F/m)
ε_r	permittivity of ethanol(F/m)
ρ	density of ethanol(kg/m^3)
σ	surface tension(N/m)
σ_0	initial surface tension(N/m)
φ	equivalent ratio

efficiency of 97%. Further they studied the performance of a combustor with liquid fuel electro-spray injection through a stack of catalytically coated grids [20].

The whole process of combustion using liquid fuel mainly includes electro-spraying, vaporization and combustion, it is quite important to understand the electro-spraying characteristics for better design and operation of micro-scale combustors. Mestel [21] investigated the steady flow in a cone-jet at high Reynolds number, when circulation occurs within the drop while the jet was fed by a surface boundary layer. Two models of the phenomena were presented with very different similarity scalings both agreed qualitatively with experiment. Experimental investigation was performed on electro sprays of liquids with low electric conductivity (heptane with different fractions of antistatic additive) in the cone-jet mode. The stable and monodisperse electro sprays could be established only within certain ranges of liquid flow rates and applied voltages [22]. The qualitative studies of jet structure and droplet formation in the electro hydrodynamic spraying were carried out. Ten modes had been distinguished and interpreted by considering the electrical and mechanical forces on the liquid jet [23,24]. The effect of pulsed voltages on electro hydrodynamic spraying in the cone-jet mode was investigated. Results showed that both the amplitude and the frequency of the pulsed voltage could affect the behavior of the spraying [25]. Deng et al. [26] successfully demonstrated the multiplexed electro spray systems with an unprecedented packing density of up to11,547 sources/cm^2. In order to generate fine droplets, electrostatic atomization was applied using nozzle and grounded ring with high voltage in between. Stable droplets of water and KCl solution were produced in oil without any surfactants [27]. Electro statically assisted sprays of butanol were established and compared with those of ethanol and heptane. The spray structure was characterized through measuring droplet sizes and velocities in a wide range of flow rates and applied voltages [28]. A high-speed camera with microscopic zoom lens had been used to visualize the deformation and breakup of charged droplets at the dripping mode. It was found that large surface tension could lead to low deformation of droplets and high voltage was necessary to make sprays transit from the dripping mode to the cone-jet mode [29].

Jaworek and krupa [30] gave the detailed description of main modes of electro hydrodynamic spraying of liquids in standard capillary-plane configuration. Chiarot et al. [31] studied experimentally the transient modes of an electrified fluid interface. There are several perfect involved reviews on the role of interfacial shear stresses [32], electro hydrodynamic spraying functioning modes [33], and the fluid dynamics of Taylor cones [34].

So far there are some researches on electro-spraying and micro-combustion, but the study on micro-combustion using electro-spraying technique is still in its infant stage. In order to enhance spraying and combustion in small-scale, a single capillary nozzle-steel ring-steel mesh configuration was placed inside a quartz glass tube with inner diameter of 16 mm. The stable combustion and flame was achieved under combined electric field. This research aimed to identify different electro-spraying modes and their operating ranges. The Taylor cone angles at the stable cone-jet mode and the specific charges at each mode were all measured. Our results will supply helpful guidance for design and operation of new small-scale combustors with high performance.

2. Experimental description

2.1. Test section

Fig. 1 shows a schematic of the present small-scale combustor. The combustor consisted of three pieces of vertical quartz glass tubes with inner diameter of 16 mm. A stainless steel ring as an extractor electrode and a stainless steel mesh as a collector electrode were connected among them by using a heat resistant adhesive. The inner diameter and outer diameter of the steel ring was 12.4 mm and 16 mm respectively. The whole steel mesh has a diameter of 16 mm and 98 round holes with a diameter of 1.0 mm in it.

A stainless steel capillary tube was used as a combustor nozzle, with an inner diameter of 0.9 mm and outer diameter of 1.2 mm. The nozzle was set at the center of the glass tube and the applied voltage to the nozzle was V_1using a Direct Current (DC) power source (Model 71030P, GENVOLT). The steel ring was arranged above the nozzle tip with vertical distance of L_1 and the applied voltage to the ring was V_2 using another DC power source. The steel mesh was arranged above the ring electrode with vertical distance of L_2 and was connected to the ground electrode with a standard resistance between them. In present study, the electric potential difference across the resistance is not bigger than 40 mV, so the electric potential on the steel mesh is near to zero. That is to say, the steel mesh can be regarded as setting to ground.

The working process of the combustor was divided into three regions. The fuel of ethanol jet was produced in the jet region, then

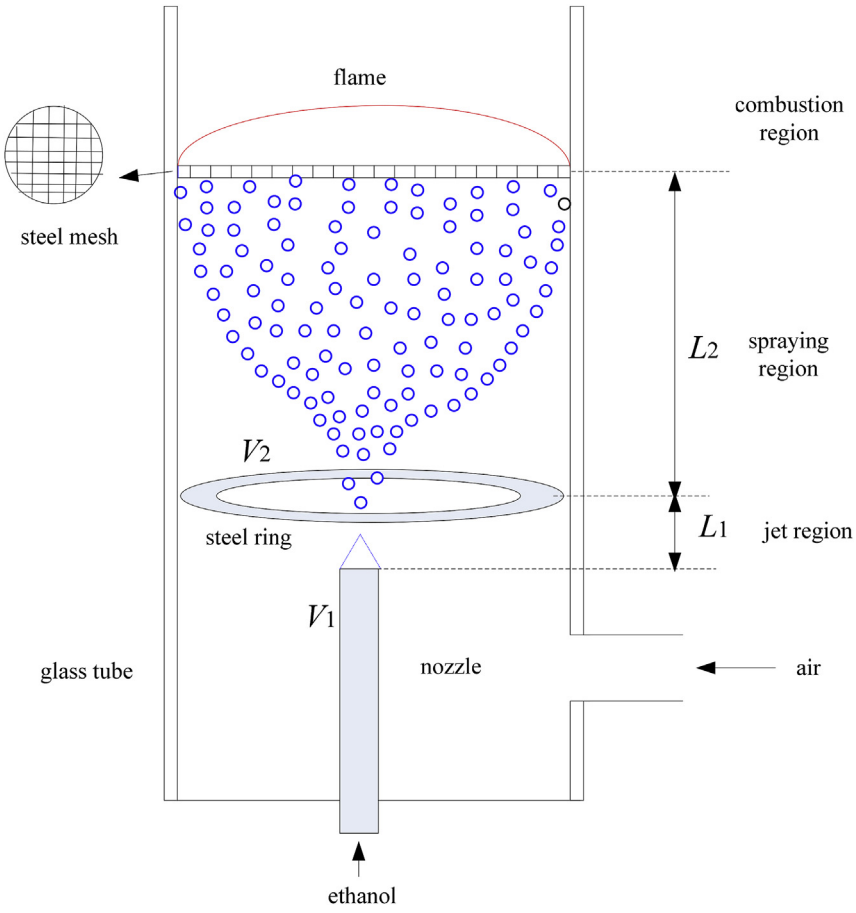

Fig. 1. Test section.

was electro-sprayed into the spraying region, and was combusted near to the mesh in the combustion region finally. The mesh was used as charged droplets collector and flame holder in present experiments.

2.2. Experimental system

Fig. 2 shows a schematic of the present experimental set-up. It consisted of a fuel supply system, a test section, an optical visualization system, a charge measurement system and a data acquisition system. The fuel was supplied to the test section by a syringe pump (KDS100, KD SCIENTIFIC) with uncertainty of 1.0%. The flow rate of liquid ethanol, Q_v, was set and accurately controlled by the syringe pump. The air was supplied to the test section by a mass flow rate controller (Brooks, 5850E) with uncertainty of 0.12%. The electro-spraying modes were visualized by the CCD camera (Jenoptik Prog Res C3 cool, 2080 × 1542 pixels, Jenoptik Group, Germany) combined with a stereo microscope (SEZ-300, Finial Company, Shenzhen, China). A green laser light was used as an illuminating light source for capturing the electro-spraying image. All images could be transferred and stored in the computer.

2.3. Specific charge measurement

The specific charge was measured using mesh target method. A standard 1 MΩ resistance was connected between the steel mesh and the ground electrode. The electric potential difference across the resistance was measured and integrally calculated by the data acquisition system (Agilent 34970A), so the specific charge, A_q can be expressed as

$$A_q = \frac{\int_0^t I dt}{\int_0^t m dt} = \frac{\int_0^t \frac{U}{R} dt}{\int_0^t \rho Q_v dt} \tag{1}$$

Where, I is current, m is mass flux of liquid fuel, t is measurement period, U is electric potential difference, $R = 1\text{M}\Omega$, ρ is density, Q_v is flow rate.

In order to improve the measurement precision, the initial current, I_0, should be considered. A very small part of ethanol was evaporated into the air and not be captured by the steel mesh should be estimated. So the specific charge was corrected by Eq. (2).

$$A_q = \frac{\int_0^t (I - I_0) dt}{\int_0^t (m - m_1) dt} \tag{2}$$

Where, I_0 is initial current, m_1 is mass flux of liquid fuel evaporated into the air.

2.4. Error analysis

The liquid fuel used in present study was pure ethanol (C_2H_5OH, with purity of 99.5%) and its physical properties were shown in Table 1. For the liquid ethanol with low conductivity,

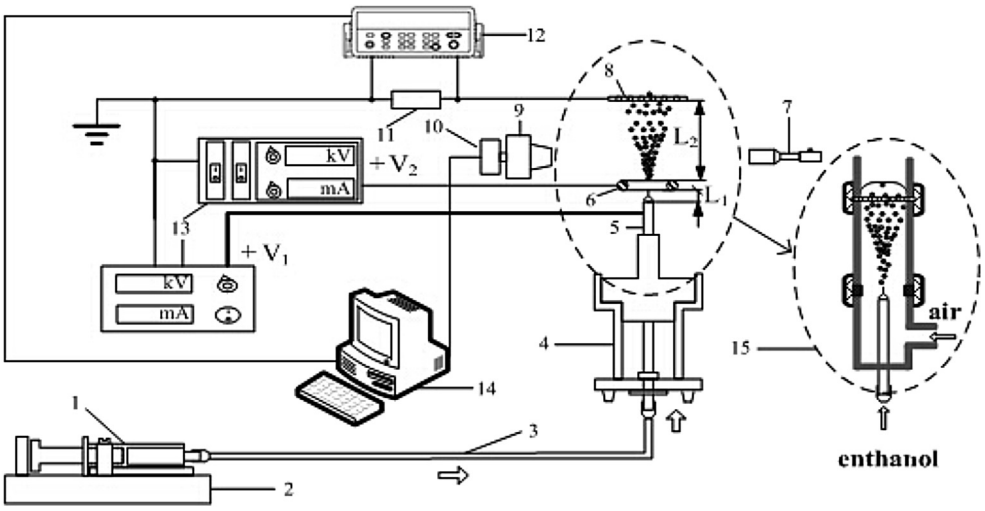

Fig. 2. The schematic diagram of the experimental set up. (1: injector, 2: syringe pump, 3: tube, 4: capillary support, 5: nozzle, 6: steel ring, 7: laser light, 8: steel mesh, 9: stereo microscope, 10: digital camera, 11: resistance, 12: data acquisition system, 13: DC power sources, 14: computer, 15: small-scale combustor).

Table 1
Physical properties of liquids.

Liquid	Density	Viscosity	Surface tension	Conductivity	Relative permittivity
	kg/m^3	mPas	N/m	S/m	–
Ethanol	789	1.16	0.022	3×10^{-4}	25

the electro-spraying system can be established based on electrostatic forces, where atomization is in principle not driven by a substantial pressure difference, unlike common pressure-driven injectors.

The experiment was conducted in the following variation ranges of operating parameters: liquid ethanol flow rate Q_v of 0.2–5.0 ml/h, applied voltage on the nozzle V_1 of 0–6.0 kV and applied voltage on the steel ring V_2 of 0–2.0 kV. The distance L_1 was 1.1 and 2.5 mm, the distance L_2 was 20 and 30 mm. According to the relationship between the indirect error and direct error, the uncertainty of indirect measurement can be estimated. Standard error analysis was performed. It was calculated that the uncertainty of specific charge was within ±7.6%.The important parameter uncertainties are summarized in Table 2.

3. Results and discussions

3.1. Modes of electro-spraying

The liquid spraying from a capillary tube nozzle at a high potential may show different forms, and was disintegrated into droplets in different ways. The classification of the electro-spraying modes is partly based on that proposed by Jaworek and Krupa [23,24,30] and Cloupeau and Prunet-Foch [33]. The modes can be classified according to the physical characteristics of the liquid at the outlet of the capillary tube nozzle and the jet behavior in its disintegration into droplets.

Table 2
Experimental uncertainties.

Parameters	Uncertainty
A_q	±7.6%
L_1	±0.02 mm
L_2	±0.02 mm
Q_v	±1.0%
V_1	±1.0%
V_2	±1.0%

The liquid jet was not formed at nozzle voltage$V_1 = 0$ and ring voltage$V_2 = 0$. Because the liquid ethanol was supplied into the nozzle at very low flow rate of 1.0 ml/h (flow velocity at the outlet was 4.37×10^{-4} m/s, and Reynolds number Re = 0.29). The interface of liquid fuel at the outlet of nozzle was nearly flat under the effects of surface tension and gravity. The kinetic energy of the liquid is less than the surface energy to create the jet surface without the external electric field.

In order to identify different spraying modes, the experiments were carried out under the fixed volume flow rate $Q_v = 1.0$ ml/h, the fixed voltage of steel ring at $V_2 = 1.0$ kV, and the distances $L_1 = 1.1$ mm, $L_2 = 30$ mm. The effect of the nozzle voltage V_1 on the spraying modes of ethanol is shown in Fig. 3. The range of the nozzle voltage V_1 varied from 0 to 5.0 kV. The typical images were selected to show different modes and the sketches of each mode were drawn to show the liquid meniscus or cone clearly.

When the nozzle voltage $V_1$was increased from 0 to 3.61 kV, the fuel in the nozzle gained more and more charges, thus the interface of liquid ethanol at the nozzle outlet became meniscus due to the effect of electric force. A typical case is shown in Fig. 3(a) at $V_1 = 3.0$ kV.

3.1.1. Pulsed-jet mode

In the range of $V_1 = 3.61$–4.19 kV, the pulsed-jet or intermittent-jet mode were observed. With the increasingV_1, the strength of electric field was increased, and beyond certain value, the liquid interface became unstable. A typical case is shown in Fig. 3(b) at $V_1 = 3.61$ kV. The whole fluid field could be divided into two regions, the jet region and the spraying region. The interface was elongated and formed a cone meniscus. A very slim jet in the center of the cone meniscus was found in the jet region between the nozzle outlet and the steel ring, and then the liquid jet was disintegrated into droplets in the spraying region between the steel ring and the steel mesh. The jet and spraying process was unstable and periodic, so it was called pulsed-jet or intermittent-jet mode in present study. The liquid ethanol was charged under the effect of electric field, and then the charges would be transferred to the steel mesh collector during the jet

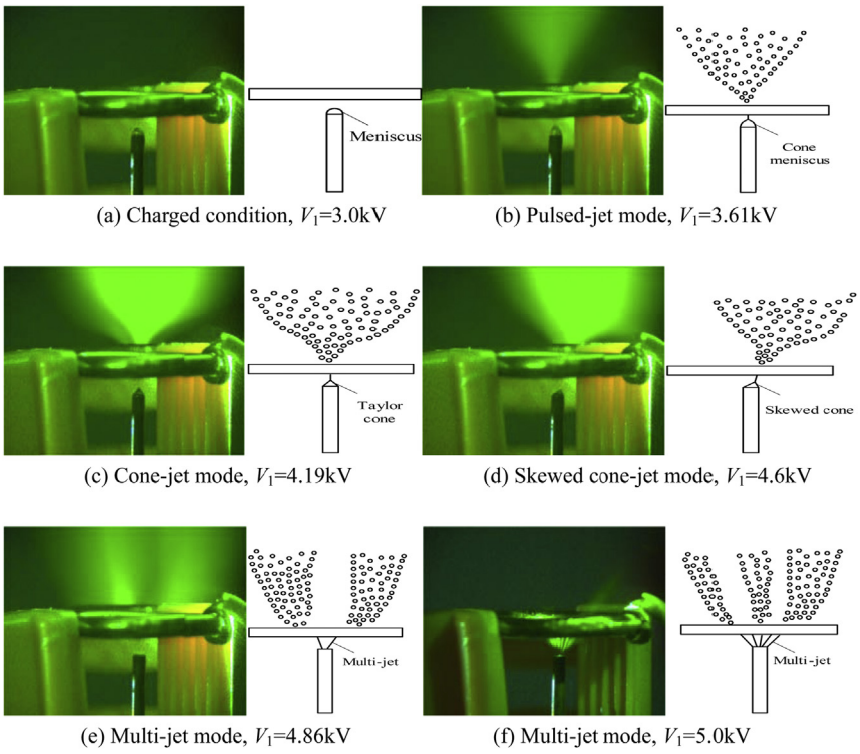

Fig. 3. The experimental snapshots and sketches for the dynamic process of electro-spraying for ethanol (Q_v = 1.0 mL/h, V_2 = 1 kV, L_1 = 1.1 mm, L_2 = 30 mm).

and spraying process. When generation rate of charges was lower than the neutralization rate, the spraying phenomenon disappeared, and the interface reverted to be flat at the outlet of the nozzle. The study of pulsating modes was reviewed by Cloupeau and Prunet-Foch [33] and was regarded as a variant of the cone-jet mode.

3.1.2. Cone-jet mode

In the range of V_1 = 4.19–4.6 kV, the stable cone-jet mode appeared. A typical case is shown in Fig. 3 (c) at V_1 = 4.19 kV. The meniscus at the liquid/air interface took the form of a Taylor cone and emitted a steady jet of liquid from its apex. The Taylor angle under this condition was 74.88°.This jet of liquid traveled a certain distance upon the cone apex before breaking up into droplets. The ethanol was sprayed very uniformly into the air. Excessive charges on the interface changed the direction of electrical force, and generated the tangential electrical force to balance the surface tension. The liquid on the surface of Taylor cone was pushed into the top of the cone by the tangential electrical force, so the jet was formed. The charge density increased greatly so that liquid was disintegrated into fine droplets. A large part of the research in recent years on electro-spraying in air involves this mode [33].

3.1.3. Skewed cone-jet mode

In the range of V_1 = 4.6–4.86 kV, the vertical jet became skewed, the Taylor cone and spraying shape were distorted greatly as shown in Fig. 3(d). According to the mode defined [33], the cone-jet system may be asymmetrical. In the limit, the skewed cone-jet may be located at the periphery of the nozzle's end. The transition from cone-jet to skewed cone-jet mode may be explained as following. The radius of curvature on the outlet of capillary nozzle is very small. When the voltage V_1 increased to a certain value, the local uninformed electric field exceeded the ionization electric field strength of air nearby the outlet, the air would be ionized and the ion wind made the jet skewed.

3.1.4. Multi-jet mode

When the voltage was increased further, the spraying shape was divided into two parts at V_1 = 4.86 kV as shown in Fig. 3(e). The jet was split with the meniscus forming tow emissive cusps. In the end, the liquid jet was divided into many parts called multi-jets at V_1 = 5.0 kV as shown in Fig. 3 (f). Several emitting sites were then established around the end of the capillary nozzle. Their number increased with the applied voltage. The multi-jet mode was regarded as a variant of cone-jet mode. Kyritsis et al. [20] pointed out the advantage of the multi-jet mode. For the same total flow rate, the sharing of the flow rate between multiple jets thus yields both finer drops and much higher emission frequencies than in the single cone-jet mode. Base on present experimental observation, when the voltage V_1 increased to a certain value, the electric field strength increased to a very high level, and that made the jet move along the electric field line. So the transition from cone-jet to multi-jet appeared.

The various spraying modes for an electro-spraying are a very complex function of fluid properties, electric field, capillary geometry, flow rate and co-flowing air. In present study, all the fluid properties and other parameters were fixed, only the electric field strength at the capillary nozzle was varied. Fig. 4 shows the calculated results of combined electric field strength (E) distribution in the jet region. Where, r is polar coordinates. When r = 0, it is at the center line of the nozzle. When the voltage V_1 = 0, the electric field strength near to zero under the effect of electric field between the steel ring and the steel mesh, and the electro-spraying were not established. And when the voltage V_1 = 4.19 kV, the combined electric field strength reach a high level, and the electro-spraying appeared. The voltage V_2 play little impact on the

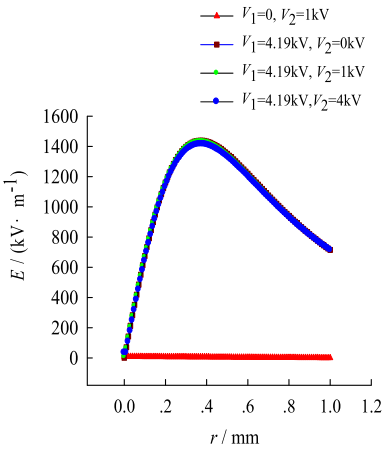

Fig. 4. The distribution of electric field strength in the jet region. (Q_v = 1.0 mL/h, L_1 = 1.1 mm, L_2 = 30 mm).

combined electric field strength. That is to say, the voltage V_1 is a key parameter for the transition from one mode to another mode in the jet region.

3.2. Operating ranges of different modes

In present study, the steel nozzle electrode, the steel ring electrode and the steel mesh ground electrode were used together to establish a combined electric flied. Four main different modes were observed during the experiments under the effects of the combined electric fields. The discontinuity of pulsed-jet mode may result in quenching of flame. The "wet-wall" phenomenon may come forth at the modes of skewed-jet and multi-jet, which may lead to incomplete combustion. So the cone-jet mode is an ideal mode, with many advantages such as stability, uniformity, hence it is the primary task for micro-scale electro-spraying combustion to operate at the cone-jet mode.

From Fig. 3 (a)-(f), it can be seen that the liquid fuel experienced four different modes along with nozzle voltage V_1 at a certain flow rate Q_v. In order to find the operating ranges of different modes, a lot of experiments were performed under different voltages, flow rates and electrode spacing. Fig. 5 shows the mode distribution with nozzle voltageV_1 and flow rate Q_v as variables. It provided easy guidance to find the suitable operating ranges of cone-jet mode to keep the combustor working well.

3.3. Effects of potential difference ΔV and distance L_1

When comparing Fig. 5(a) and (d), it can be seen that the boundaries of four modes all moved upside along with increasing the steel ring electrode voltage V_2, i.e. the nozzle voltage V_1 needed to be increased accordingly in order to achieve the same mode. The same trend could be found when comparing Fig. 5 (b) and (c). The potential difference $\Delta V = V_1 - V_2$was defined and used to consider the effect on electro-spraying modes. At L_1 = 1.1 mm, it was found that pulsed-jet appeared in the range of ΔV = 2.2–2.6 kV, cone-jet in the range of ΔV = 2.6–3.4 kV, skewed cone-jet in the range of ΔV = 2.6–3.4 kV, multi-jet in the range of ΔV = 3.1–3.7 kV.When comparing Fig. 5 (a) and (e), the boundaries of four modes all moved upside along with L_1increasing from 1.1 mm to 2.5 mm, therefore it could be concluded that the driving force of electro-spraying in present system mainly came from the electrostatic induction field between the nozzle and the steel ring electrode in the jet region.

By assuming the ethanol as ideal fluid, ignoring the effect of charge of ethanol surface on electric field strength, the electric force per jet surface can be calculated by:

$$F = \frac{1}{2}(\varepsilon_0 - \varepsilon_r)\left(E_a^2 + \frac{\varepsilon_0}{\varepsilon_r}E_r^2\right) \tag{3}$$

Where, E_a and E_r are axial and radial electric field strength respectively. ε_0, ε_r are permittivity of air and ethanol respectively.

The decrement of surface tension due to induced charge is expressed as

$$\Delta\sigma = \frac{Q_v^2}{(8\pi)^2\sigma_0 r^3} \tag{4}$$

Where σ_0 is initial surface tension, Q_v is flow rate, and r is radius of jet.

During the motion of ethanol jet, several forces will act on it, including the internal pressure P_{in}, surface tension σ_0-$\Delta\sigma$, electric field force F, and external pressure P_{ex}.

$$P_{in} = \frac{\sigma_0 - \Delta\sigma}{r} + F + P_{ex} \tag{5}$$

When $P_{in} = P_{ex}$, the radius will reach its critical value.

$$r_{cr} = -\frac{\sigma_0 - \Delta\sigma}{F} \tag{6}$$

So the critical radius decreases with increasing the electric field strength, which can enhance disintegration into droplets of the liquid ethanol.

3.4. Effects of voltage V_2 and distance L_2

When comparing Fig. 5 (a) and (d), the working range of flow rates were enlarged along with increasing V_2 from 1.0 kV to 2.0 kV. The upper limit of flow rate increased from 2.8 ml/h to 3.6 ml/h (keeping L_1 = 1.1 mm and L_2 = 30 mm). The similar conclusion could be drawn comparing Fig. 5 (b) and (c). The upper limit of flow rate increased from 1.4 ml/h to 3.4 ml/h (keeping L_1 = 1.1 mm and L_2 = 20 mm), therefore the voltage V_2 could enlarge the working range of ethanol electro-spraying.

During the experimental process, it was found that the spraying shape changed greatly when the distance $L_2$was increased from 20 mm to 30 mm. The variation was shown in Fig. 6 (a) and (b), so the distance L_2 could affect obviously the electro-spraying and its uniformity.

Fig. 6(c) shows another important phenomenon which was observed that the electro-spraying shape changed greatly, and a lot of liquid droplets reverted to the steel ring electrode when the steel mesh was removed from the experimental system. Thus, it could be inferred that the electric field between the steel ring and the steel mesh provided driving force for the motion of liquid droplets in the spraying region, and the steel mesh is a crucial component for the directional movement and capture of liquid droplets.

3.5. Taylor angles at the cone-jet mode

The cone-jet mode is a perfect electro-spraying mode and the Taylor angle is a unique and complex phenomenon, resulting from the balance among viscous force, gravity, pressure, surface tension and electric force. It was shown theoretically that a conical interface between two fluids can exist in equilibrium in an electric field, but only when the cone has a semi-vertical angle 49.3° [35].

In present study, the images of electro-spraying at stable cone-jet mode were captured by CCD camera combined with stereo

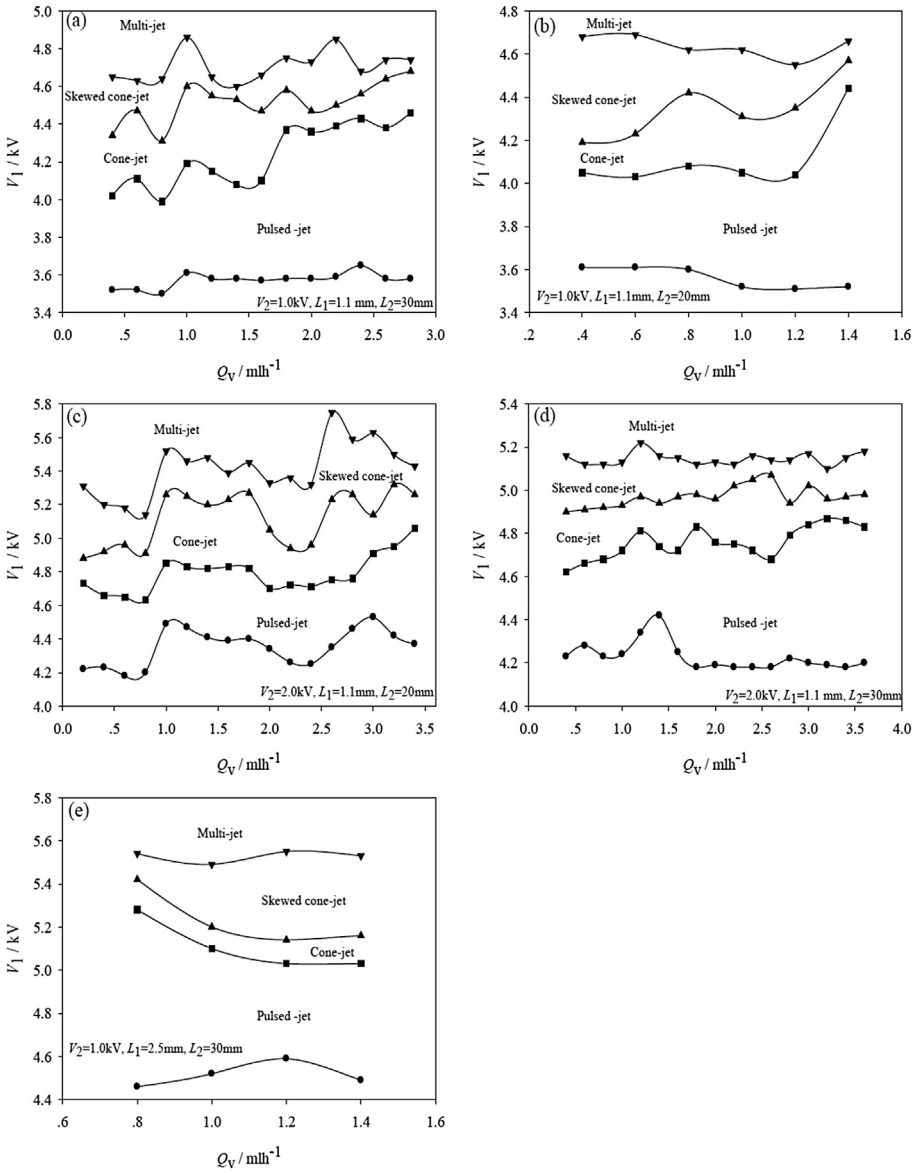

Fig. 5. The operating ranges of different spraying modes for ethanol.

microscope. The Taylor angles were measured by post-processing software based on these images. Table 3 shows the Taylor angles of ethanol at $V_2 = 1.0$ kV, $L_1 = 1.1$ mm, $L_2 = 30$ mm. All these Taylor angles are in the range of 75.18°–82.45°, much smaller than the theoretical value 98.6° of water [35].

3.6. Specific charge

The specific charge is one of important parameters to quantify the electro-spraying characteristics. The present experimental results were shown in Fig. 8 and it was found that there were different trends at different modes. The specific charges gradually increased along with the steel ring electrode voltage V_1 at the pulsed-jet mode. When reaching the lower limit of cone-jet mode, the specific charge increased greatly. From Fig. 7 (a), the specific charge increased from 0.03006 C/kg to 0.07953 C/kg at the transition region of $V_1 = 4.11$–4.19kV with the flow rate of 1.0 ml/h. From Fig. 7 (b), the specific charge increased from 0.02975 C/kg to 0.09103 C/kg at the transition region of $V_1 = 4.28$–4.36 kV with the flow rate of 2.0 ml/h. At the cone-jet mode, the specific charges reached maximum values of 0.09389 C/kg and 0.1263 C/kg in Fig. 7 (a) and (b) respectively. Those were the optimum values in present experimental system. At skewed cone-jet and multi-jet regions, the specific charges gradually decreased.

The variation trends in Fig. 7 could be explained by the induction charge injection methods and residence time of ethanol in the electric field between the nozzle electrode and the steel ring electrode. The induction charge injection controlled the process at the modes of pulsed-jet and cone-jet. When the voltage V_1 was low, the axial velocity of liquid jet and droplet was relatively low, the residence time was quite long so that the specific charge increased with the increasing V_1. When the voltage V_1 increased, the electric field strength between the nozzle and ring electrodes was enhanced gradually, the velocities of jet and droplet were increased, so the induction charge injection was weakened due to the reduction of residence time. At skewed cone-jet and multi-jet regions, corona condition emerged, and partial charges were discharge into the air with residual charges still in the spraying. When voltage V_1 increased to a certain extent, the corona condition dominated the charge

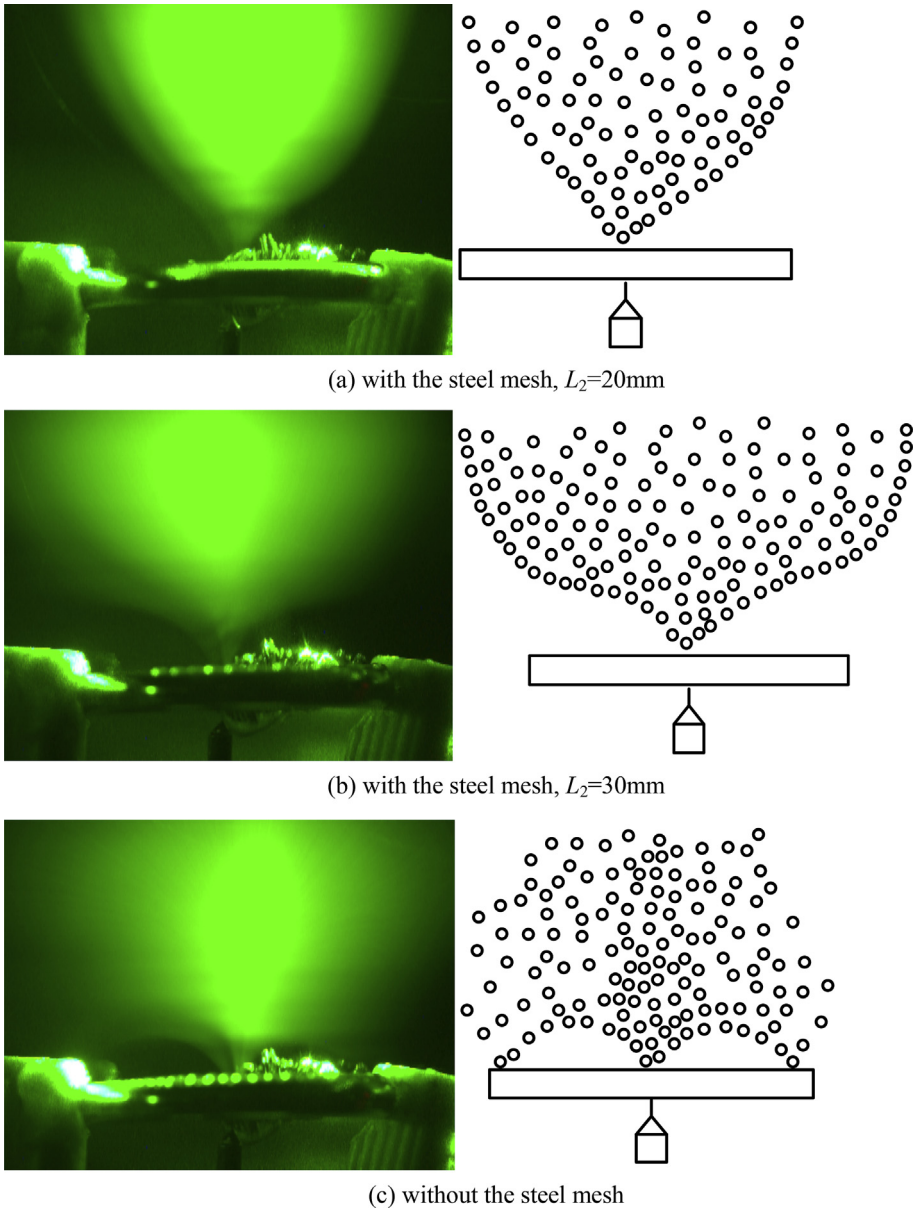

(a) with the steel mesh, L_2=20mm

(b) with the steel mesh, L_2=30mm

(c) without the steel mesh

Fig. 6. Experimental snapshots and sketches for three different shapes in the spraying region(Q_v = 2 mL/h, V_1 = 4.8 kV, V_2 = 2 kV, L_1 = 1.1 mm).

Table 3
Taylor angles at the cone-jet mode (V_2 = 1.0 kV, L_1 = 1.1 mm, L_2 = 30 mm).

Flow rate Q_v (ml/h)	Voltage V_1 (kV)	Taylor angle (°)	Flow rate Q_v (ml/h)	Voltage V_1 (kV)	Taylor angle (°)
1.0	4.24	76.86	1.2	4.44	77.08
	4.44	79.70		4.54	77.91
	4.54	80.31		4.72	82.45
1.4	4.13	77.81	1.6	4.13	76.41
	4.24	79.20		4.24	79.39
	4.28	77.04		4.37	78.66
1.8	4.37	75.18	2.0	4.0.37	75.27
	4.44	77.47		4.44	76.32
	4.54	81.95		4.47	77.82

injection process, so the specific charges decreased and kept almost constant at the skewed cone-jet and multi-jet modes compared with cone-jet mode. Thus, it can be inferred that the measurement of specific charge was another important method to identify different electro-spraying modes of liquid ethanol in small-scale system.

3.7. Flame image

A series of combustion experiments were carried out based on present test section and experimental system using ethanol as fuel. Fig. 8 shows a typical flame image for a combustion case under the conditions of flow rate Q_v = 5.0 mL/h, voltage on the nozzle V_1 = 4.19 kV, voltage on the steel ring V_2 = 1.0 kV, distance from top of the nozzle to the steel ring L_1 = 1.1 mm, distance from the steel ring to the steel mesh L_2 = 30 mm, and equivalence ratio φ = 1.6. The combustion experiments were conducted at the ambient temperature of 290 K, and the relative humidity of 61.2%.

The liquid ethanol was accurately controlled by a syringe pump, and the air was accurately controlled by a mass flow controller. Under the effect of combined electric field established by the nozzle, the steel ring and the steel mesh, the ethanol flow was

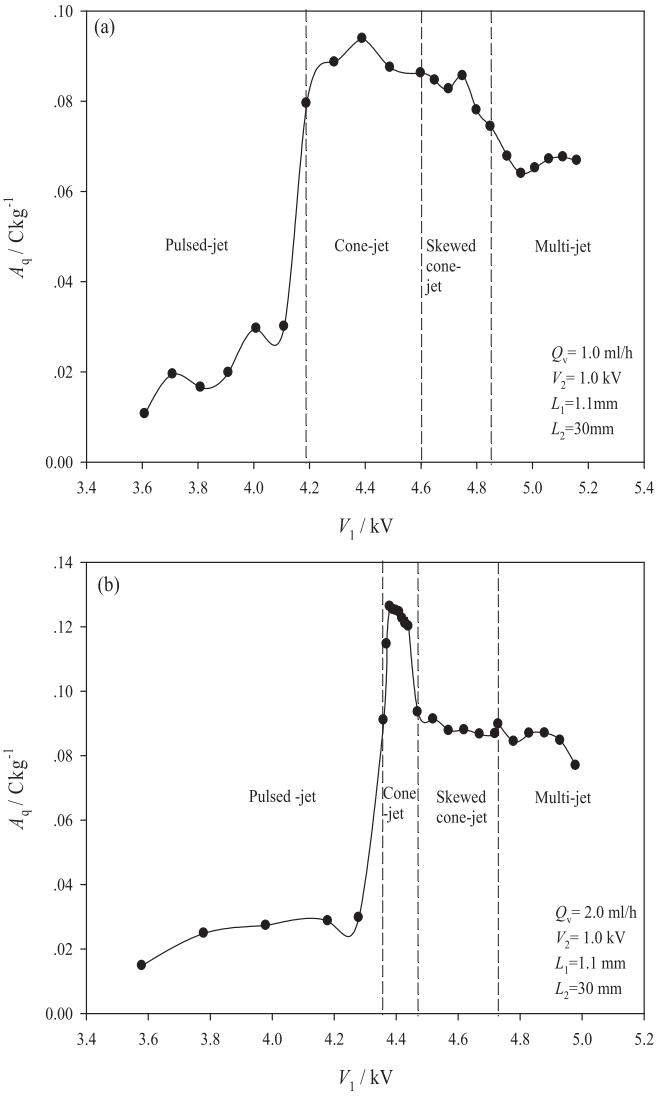

Fig. 7. The variation of specific charge along the nozzle voltage V_1 at different spraying modes.

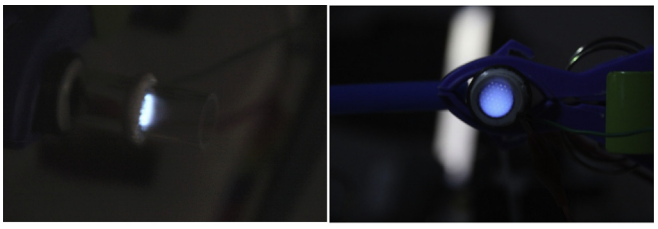

(a) side view (b) top view

Fig. 8. A typical flame images. (Q_v = 5.0 mL/h, V_1 = 4.19 kV, V_2 = 1.0 kV, L_1 = 1.1 mm, L_2 = 30 mm, φ = 1.6).

formed into jets in the jet region and breaking-up into droplets uniformly in the spraying region. The very small spraying liquid droplets were collected by the steel mesh. At the initial stage, the glass tube was preheated by an external heater that was located near to the steel mesh. After the ethanol was ignited, the combustion was self-sustained and the external heater was no longer needed. The flame existed on the steel mesh with a blue luminosity, implying no soot formation. The flame looked like a slice on the steel mesh which has the function of flame holder. The stable combustion and flame lasted till all the fuel was consumed.

The typical combustion case is used to show the success of applying electro-spraying technology in the small-scale combustion system.

4. Conclusions

In present study, a novel small-scale combustor with a steel nozzle, a steel ring extractor, and a steel mesh was built up, and a series of experiments on electro-spraying using liquid ethanol as fuel were carried out. Some main conclusions can be drawn as following.

(1) A typical stable burning combustion condition was used to show the success of applying electro-spraying technology in present small-scale combustion system.
(2) The modes of pulsed-jet, cone-jet, skewed cone-jet, and multi-jet were observed by optical visualization method.
(3) The operating ranges of different electro-spraying modes for ethanol were divided into several regions based on present experimental results.
(4) The driving force in jet region in present system mainly came from the electrostatic induction field between the nozzle and the steel ring.
(5) The electric field between the steel ring and the steel mesh supplied driving force for the motion of liquid droplets in the spraying region, and the steel mesh was a key component for the directional movement and capture of liquid droplets.
(6) Taylor angles measured in present experiments at cone-jet mode are in the range of 75.18°–82.45°.
(7) The specific charges of electro-spraying ethanol reached maximum value at the cone-jet mode, which supplied another suitable tool to identify different modes.

Future work by the authors shall include combustion characteristics using electro-spraying technique and its relationship to operating modes. The velocity field and droplet size should be measured. Utilizing key dimensionless groups to describe the different modes would also be required. A future paper by the authors will provide a detailed report of combustion characteristics, such as flame stability limits, flame temperature, heat efficiency, and combustion efficiency and so on.

Acknowledgements

The authors gratefully acknowledge the National Natural Science Foundation of China (51376066, 51406050) and the Special Foundation of Pearl River New Star of Science and Technology in Guangzhou City (2012J2200002).

References

[1] L. Yuliati, T. Seo, M. Mikami, Liquid-fuel combustion in a narrow tube using an electro spray technique, Combust. Flame 159 (2012) 462–464.
[2] M. Mikami, Y. Maeda, K. Matsui, et al., Combustion of gaseous and liquid fuels in meso-scale tubes with wire mesh, Proc. Combust. Inst. 34 (2013) 3387–3394.
[3] H. Wang, A.V. Mamishev, Heat transfer correlation models for electro spray evaporative cooling chambers of different geometry types, Appl. Therm. Eng. 40 (2012) 91–101.
[4] H. Wang, N.E. Jewell-Larsen, A.V. Mamishev, Thermal management of microelectronics with electro static fluid accelerators, Appl. Therm. Eng. 51 (2013) 190–211.
[5] W.W. Deng, A. Gomez, Electrospray cooling for microelectronics, Int. J. Heat. Mass Tran 54 (2011) 2270–2275.
[6] M.M. Hohman, Electro spinning and electrically forced jets. I. Stability theory, Phys. Fluids 13 (2001) 2201–2220.

[7] M.M. Hohman, Electro spinning and electrically forced jets. II. Applications, Phys. Fluids 13 (2001) 2221–2236.
[8] O. Wilhelm, Electro Hydrodynamic Spraying –Transport, Mass and Heat Transfer of Charged Droplets and Their Application to the Deposition of Thin Functional Films, Ph.D. Dissertation, Swiss Federal Institute of Technology, Zurich, 2004.
[9] A. Attoui, J. Fernandez-Garcia, J. Cuevas, et al., Charge evaporation from nanometer polystyrene aerosols, J. Aerosol Sci. 55 (2013) 149–156.
[10] J. Fernandez de la Mora, Ionization of vapor molecules by an electro spray cloud, Int. J. Mass Spectrom. 300 (2011) 182–193.
[11] R. Juraschek, F.W. Rollgen, Pulsation phenomena during electro spray ionization, Int. J. Mass Spectrom. 177 (1998) 1–15.
[12] A. Kourmatzis, J.S. Shrimpton, Electrical and transient atomization characteristics of a pulsed charge injection atomizer using electrically insulating liquids, J. Electrost. 69 (2011) 157–167.
[13] A. Kourmatzis, J.S. Shrimpton, Design and charge injection characteristics of an electrostatic dielectric liquid pulsed atomizer, J. Electrost. 70 (2012) 249–257.
[14] A. Kourmatzis, J.S. Shrimpton, Electro hydrodynamic inter-electrode flow and liquid jet characteristics in charge injection atomizers, Exp. Fluids 55 (2014) 1688.
[15] G. Bagheri, S.E. Hosseini, M.A. Wahid, Effects of bluff body shape on the flame stability in premixed micro-combustion of hydrogen-air mixture, Appl. Therm. Eng. 67 (2014) 266–272.
[16] B. Khandelwal, A.A. Deshpande, S. Kumar, Experimental studies on flame stabilization in a three step rearward facing configuration based micro channel combustor, Appl. Therm. Eng. 58 (2013) 363–368.
[17] A. Rosato, S. Sibilio, Calibration and validation of a model for simulating thermal and electric performance of an internal combustion engine-based micro-cogeneration device, Appl. Therm. Eng. 45–46 (2012) 79–98.
[18] Y.H. Gan, J.L. Xu, Y.Y. Yan, et al., A comparative study on free jet and confined jet diffusion flames of liquid ethanol from small nozzles, Combust. Sci. Technol. 186 (2014) 120–138.
[19] D. Kyritsis, I. Guerrero-arias, S. Roychoudhury, et al., Mesoscale power generation by a catalytic combustor using electro sprayed liquid hydrocarbons, Proc. Combust. Inst. 29 (2002) 965–972.
[20] D. Kyritsis, B. Coriton, F. Faure, et al., Optimization of a catalytic combustor using electrosprayed liquid hydrocarbons for mesoscale power generation, Combust. Flame 139 (2004) 77–89.
[21] A. Mestel, The electro hydrodynamic cone-jet at high Reynolds number, J. Aerosol Sci. 25 (1994) 1037–1047.
[22] K.Q. Tang, A. Gomez, Monodisperse electro sprays of low electric conductivity liquids in the cone-jet mode, J. Colloid Interf. Sci. 184 (1996) 500–511.
[23] A. Jaworek, A. Krupa, Jet and drops formation in electro hydrodynamic spraying of liquids, A systematic approach, Exp. Fluids 27 (1999) 43–52.
[24] A. Jaworek, A. Krupa, Classification of the modes of EHD spraying, J. Aerosol Sci. 30 (1999) 873–893.
[25] J. Li, On the stability of electro hydrodynamic spraying in the cone-jet mode, J. Electrost. 65 (2007) 251–255.
[26] W.W. Deng, C.M. Waits, B. Morgan, et al., Compact multiplexing of monodisperse electro sprays, J. Aerosol Sci. 40 (2009) 907–918.
[27] B. Sadri, B. Hokmabad, E. Esmaeilzadeh, et al., Experimental investigation of electro sprayed droplets behavior of water and KCl aqueous solutions in silicone oil, Exp. Therm. Fluid Sci. 36 (2012) 249–255.
[28] M. Agathou, D. Kyritsis, Electrostatic atomization of hydrocarbon fuels and bio-alcohols for engine applications, Energ. Convers. Manage 60 (2012) 10–17.
[29] Y.P. Huo, J.F. Wang, W.L. Mao, et al., Measurement and investigation on the deformation and air-assisted breakup of charged droplet, Flow. Meas. Instrum. 27 (2012) 92–98.
[30] A. Jaworek, A. Krupa, Main modes of electro hydrodynamic spraying of liquids, in: Third Int. Conf. On Multiphase Flow, Lyon, France, June 8-12, 1998.
[31] P.R. Chiarot, S.I. Gubarenko, R.B. Mrad, et al., On the pulsed and transitional behavior of an electrified fluid interface, J. Fluids Eng. 131 (2009) 091202.
[32] J.R. Melcher, G.I. Taylor, Electro hydrodynamics: a review of the role of interfacial shear stresses, Annu. Rev. Fluid Mech. 1 (1969) 111–146.
[33] M. Cloupeau, B. Prunet-Foch, Electro hydrodynamic spraying functioning modes: a critical review, J. Aerosol Sci. 5 (1994) 1021–1036.
[34] J. Fernandez de la Mora, The fluid dynamics of Taylor cones, Annu. Rev. Fluid Mech. 39 (2007) 217–243.
[35] G. Taylor, Disintegration of water drops in an electric field, Proc. R. SocA 280 (1964) 383–397.